Appl Phys B (2008) 93: 837–847
DOI 10.1007/s00340-008-3216-y

Applied Physics B
Lasers and Optics

Intermodulation distortion of the single-mode laser-diode

M. Schetzen · R. Yildirim · F. Çelebi

Received: 17 March 2008 / Revised version: 29 April 2008 / Published online: 21 October 2008

Abstract A detailed study of laser-diode intermodulation distortion (IMD) using the Volterra model that was developed for the single-mode laser-diode with optoelectronic feedback is presented in this paper. The IMD is analyzed by analyzing the amplitudes of the output sinusoids of various frequencies resulting from an input which is the sum of two sinusoids. The sinusoids at all frequencies due to the first-, second-, and third-order Volterra operators were determined and are discussed in this paper. The ones with frequencies which are not used in practical applications are included since, even though they are not in the pass-band of the first-order operator, they still can possibly effect system performance.

PACS 42.55Px · 42.65Ky

1 Introduction

In this paper, we use the system theory of the single-mode laser-diode which was developed and discussed in [1] and also reprinted in Appendix C of [2] in which the laser-diode was shown to be a nonlinear low-pass system which achieves a band-pass characteristic as a consequence of feedback. Some applications of the theoretical model developed in [1, 2] are reported in [3] and also reprinted in Appendix C of [2]. In addition to those discussed in [2, 3], the theoretical model also can be used to determine desirable values of the laser-diode parameters as well as to determine and analyze the laser-diode response to any given excitation. Another application is a detailed study of distortion and its sources. This is studied in this paper by an analysis of intermodulation distortion (IMD) by using the Volterra model of the single-mode laser-diode with electronic feedback which was developed and analyzed in [1, 2].

Laser-diode studies in recent years have focused on the effects of optical and electronic feedback effects [4–15]. The effect of nonlinear distortion is often discussed in terms of the output harmonics resulting from an input sinusoidal waveform. Another method of discussing nonlinear distortion is in terms of the output amplitudes of the sinusoids of the various frequencies produced by an input consisting of a sum of sinusoids. This more closely demonstrates the nonlinear distortion effect in practical application. Classically, this nonlinear distortion was observed by applying an amplitude modulated sinusoid and noting the effective change in the amplitude modulation of the resulting output sinusoid with the same frequency as that of the input sinusoid. This type of distortion was thus referred to as intermodulation distortion (IMD). In this paper, the IMD of the laser-diode is studied by analyzing the amplitudes of the output sinusoids of various frequencies resulting from an input which is the sum of two sinusoids. The output sinusoidal amplitudes resulting from the first-, second-, and third-order Volterra operators were determined analytically using the nonlinear model developed in [1, 2] and the equations were programmed using MatLab. The sinusoids at all frequencies due to the first-, second-, and third-order Volterra operators were determined and are discussed in this paper. The ones

M. Schetzen (✉)
Northeastern University, Boston, USA
e-mail: schetzen@ece.neu.edu

R. Yildirim
Gazi University, Ankara, Turkey
e-mail: remzi@gazi.edu.tr

F. Çelebi
Ankara University, Ankara, Turkey
e-mail: fcelebi@eng.ankara.edu.tr

with frequencies which are not used in practical applications are included since, even though they are not in the pass-band of the first-order operator, they still can possibly effect system performance.

2 The Volterra model

In the Volterra model, the laser-diode photon population response, $p(t)$, to the current input $i(t)$ is expressed as the sum

$$p(t) = p_0 + \sum_{m=0}^{\infty} p_m(t) \tag{1}$$

in which $p_m(t)$ is the photon population response of the mth-order Volterra operator. The charge carrier population number, $n(t)$, is also expressed as the sum

$$n(t) = n_0 + \sum_{m=0}^{\infty} n_m(t) \tag{2}$$

in which $n_m(t)$ is the charge carrier population number response of the mth-order Volterra operator. The IMD is determined in this paper for the injection current input

$$i(t) = I_1 \cos(\omega_1 t + \delta_1) + I_2 \cos(\omega_2 t + \delta_2) \tag{3}$$

in which I_1 and I_2 are the amplitudes of the sinusoids with frequencies ω_1 and ω_2 and the phases δ_1 and δ_2, respectively. The IMD was determined for a laser-diode with electronic feedback in which the feedback current is numerically equal to the photon output multiplied by a constant, g, and delayed by t_0 seconds so that the feedback current added to the injection current input is $gp(t - t_0)$. The first three Volterra operators for the laser-diode with electronic feedback, Z_n, given in [1, 2] are described below.

2.1 The Volterra operator block diagrams

The first-order Volterra operator, Z_1, is a linear system with the transfer function

$$Z_1(j\omega) = \frac{H_1(j\omega)}{1 + H_1(j\omega)G_1(j\omega)} \tag{4}$$

in which

$$H_1(j\omega) = \frac{B_0}{q} \frac{1}{(D_0 - \omega^2) + jD_1\omega} \tag{5}$$

and

$$G_1(j\omega) = ge^{-j\omega t_0} \tag{6}$$

A block diagram of Z_2, the second-order Volterra operator of the laser-diode with electronic feedback, is shown in Fig. 1. In the figure, H_2 is the second-order Volterra operator of the laser-diode without feedback; Fig. 2 is a block diagram of H_2. The transfer functions of the linear systems in the block diagrams are

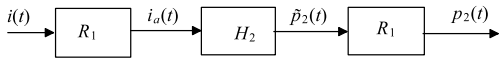

Fig. 1 The operator Z_2

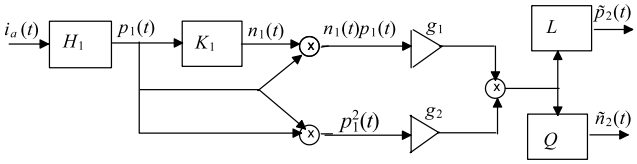

Fig. 2 The operator H_2

$$R_1(j\omega) = \frac{1}{1 + H_1(j\omega)G_1(j\omega)} \tag{7}$$

$$L(j\omega) = \frac{j\omega - \frac{\beta\Gamma - 1}{\tau n}}{(D_0 - \omega^2) + jD_1\omega} \tag{8}$$

$$Q(j\omega) = \frac{1}{B_0}\left[\frac{(j\omega + B_1)(j\omega - \frac{(\beta\Gamma - 1)}{\tau n})}{(D_0 - \omega^2) + j\omega D_1} - 1\right] \tag{9}$$

The amplifier gains in Fig. 2 are

$$\begin{aligned} g_1 &= \Gamma A[1 - 2\hat{\epsilon}P_0] \quad \text{and} \\ g_2 &= -\Gamma A\hat{\epsilon}[N_0 - N_{\text{tr}}] \end{aligned} \tag{10}$$

Since the linear systems H_1 in Fig. 2 and the first R_1 in Fig. 1 are connected in tandem, the transfer function of the tandem connection is the product of the two individual transfer functions which is

$$R_1(\omega)H_1(\omega) = \frac{H_1(j\omega)}{1 + H_1(j\omega)G_1(j\omega)} = Z_1(j\omega) \tag{11}$$

in which $Z_1(j\omega)$ is given by (4). In the block diagram, $n_1(t)$ is the response of the linear system K_1 to the input $p_1(t)$ in which

$$K_1(j\omega) = \frac{1}{B_0}(B_1 + j\omega) \tag{12}$$

The amplifier gains in Fig. 2 are

$$\begin{aligned} g_1 &= \Gamma A[1 - 2\hat{\epsilon}P_0] \quad \text{and} \\ g_2 &= -\Gamma A\hat{\epsilon}[N_0 - N_{\text{tr}}] \end{aligned} \tag{13}$$

The constants B_n and D_n are derived in [1, 2] in terms of the other above constants which are diode parameters. The parameter values used in this paper for the numerical determination of the laser-diode IMD are those given in Hassine et al. [16] and also listed in [1, 2].

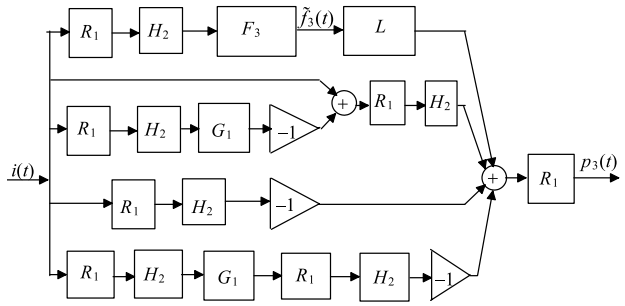

Fig. 3 The operator Z_3

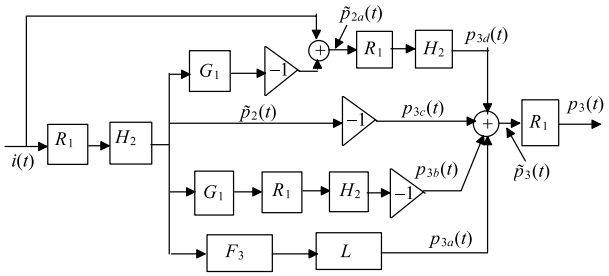

Fig. 4 Equivalent operator Z_3

From Fig. 6 of [1, 2], a block diagram of Z_3, the third-order Volterra operator of the laser-diode with electronic feedback, is shown in Fig. 3. In the figure, H_2 is the second-order Volterra operator of the laser-diode without feedback shown in Fig. 2 above. The top branch is H_3, the third-order Volterra operator of the laser-diode without feedback. In that branch, F_3 is the function for which

$$\tilde{f}_3(t) = 2\Gamma A\hat{\varepsilon}[N_{\mathrm{tr}} - N_0]p_1(t)\tilde{p}_2(t) - [\Gamma A\hat{\varepsilon}]p_1^2(t)n_1(t) + \Gamma A[1 - 2\hat{\varepsilon}P_0]\big[n_1(t)\tilde{p}_2(t) + p_1(t)\tilde{n}_2(t)\big] \quad (14)$$

The time functions in (14) are those labeled in Fig. 2. The computation required to determine $p_3(t)$ is reduced somewhat by the equivalent block diagram of the operator Z_3 shown in Fig. 4 which is obtained by noting that the time functions are identical at some places in Fig. 3.

2.2 Computer simulation

The block diagrams shown could be simulated on a computer and the responses for any input could be observed and analyzed experimentally. However, for a study of IMD, the outputs for the input given by (3) were determined analytically and the equations were programmed using MatLab.

From (4), the photon population response of the first-order Volterra kernel due to the injection current input given by (3) is

$$p_1(t) = FP_1\cos\big[\omega_1 t + \delta_1 + \measuredangle Z_1(j\omega_1)\big] + FP_2\cos\big[\omega_2 t + \delta_2 + \measuredangle Z_1(j\omega_2)\big] \quad (15a)$$

in which

$$FP_1 = I_1\big|Z_1(j\omega_1)\big| \quad \text{and} \quad FP_2 = I_1\big|Z_1(j\omega_2)\big| \quad (15b)$$

In (15), $|Z_1(j\omega)|$ is the magnitude of $Z_1(j\omega)$ and $\measuredangle Z_1(j\omega)$ is the angle of $Z_1(j\omega)$.

From Figs. 1 and 2, the block diagrams, the photon population response of the second-order Volterra kernel, Z_2, due to the injection current input given by (3), was determined analytically to be

$$\begin{aligned} p_2(t) = {} & SPR_0 + SPR_1\cos[2\omega_1 t + SPR_1 A] \\ & + SPR_2\cos[2\omega_2 t + SPR_2 A] \\ & + SPR_3\cos\big[(\omega_2 - \omega_1)t + SPR_3 A\big] \\ & + SPR_4\cos\big[(\omega_2 + \omega_1)t + SPR_4 A\big] \end{aligned} \quad (16)$$

Note that the expression is the sum of sinusoids with the five sum and difference frequencies 0, $2\omega_1$, $2\omega_2$, $\omega_2 - \omega_1$, and $\omega_2 + \omega_1$. The expressions for the amplitudes, SPR_n, and the phases, $SPR_n A$, were obtained analytically and programmed using Matlab to obtain the graphs to be discussed below.

Using Fig. 4, the photon population response of the third-order Volterra kernel, Z_3, due to the injection current input given by (3), was determined analytically to be

$$\begin{aligned} p_3(t) = {} & TPR_1\cos[\omega_1 t + TPR_1 A] \\ & + TPR_3\cos[3\omega_1 t + TPR_3 A] \\ & + TPR_5\cos[\omega_2 t + TPR_5 A] \\ & + TPR_7\cos[3\omega_2 t + TPR_7 A] \\ & + TPR_{11}\cos\big[(2\omega_2 + \omega_1)t + TPR_{11} A\big] \\ & + TPR_{13}\cos\big[(2\omega_1 + \omega_2)t + TPR_{13} A\big] \\ & + TPR_{17}\cos\big[(2\omega_2 - \omega_1)t + TPR_{17} A\big] \\ & + TPR_{19}\cos\big[(2\omega_1 - \omega_2)t + TPR_{19} A\big] \end{aligned} \quad (17)$$

Note that the expression is the sum of sinusoids with the frequencies ω_1, $3\omega_1$, ω_2, $3\omega_2$, $(2\omega_2 + \omega_1)$, $(2\omega_1 + \omega_2)$, $(2\omega_2 - \omega_1)$, and $(2\omega_1 - \omega_2)$. The rather long expressions for the amplitudes TPR_n and phases $TPR_n A$ were obtained from Fig. 4 analytically and programmed using Matlab to obtain the graphs discussed below. In the computation of the third-order response, there are several other frequencies that arise whose sinusoidal amplitudes are actually zero. However, the computation results in non-zero amplitudes due to finite word length. Those sinusoids are easily identified since their amplitudes are more than 100 dB below those of the third-order Volterra operator outputs. Further, their amplitudes do not vary as the third power of the total input amplitude of $i(t)$ as must be the case for the output of a third-order Volterra operator. It should be noted though that the

amplitude variation of a given IMD component with I_1 or I_2 will depend on the paths through the block diagram from which the given IMD component is formed. Whatever the path, it is seen that the linear systems in the block diagrams have a significant effect on the graph of the IMD component versus frequency. We thus begin with a discussion of the first-order photon response.

For convenience, in our discussion we define the normalized radian frequency as $\omega_n = \omega \cdot t_0$, the complex frequency as $s = \sigma + j\omega$, and the normalized complex frequency as $s_n = s \cdot t_0$.

3 The first-order Volterra operator response

As a consequence of linearity, it is seen from (15) that the first-order photon sinusoidal response at frequency ω_2 is dependent only on the input current sinusoid at that frequency and its amplitude is determined by $|Z_1(j\omega_2)|$ which, from (4), (5), and (6), is dependent on the feedback parameters g and t_0. With no feedback, the poles of the system function, $Z_1(s)$, are on or close to the σ axis and travel away from it and toward the ω axis with increasing feedback resulting in a band-pass characteristic of the laser-diode. As shown in [1, 2], a lower bound of the largest value of the gain, g, for which the pole is to the left of the ω axis so that the system is stable is $g_0 = \frac{qD_1}{B_0 t_0}$. We thus express the gain as $g = Kg_0$.

For values of K near zero, the laser-diode has a low-pass characteristic. For larger values of K, the laser-diode has a band-pass characteristic. For such values of K, there are several poles in the s-plane, but there is only one dominant pole in the pass-band region. The dominant pole position thus was determined from the graph of $|Z_1(j\omega_n)|$ vs. ω_n from which the pole position can be approximately determined from the graph as

$$s_n = \sigma_n + j\omega_n \approx -\left[\frac{1}{2}\ 3\text{ dB bandwidth}\right] + j[\text{frequency of maximum gain}]$$

In this manner, the locus of the dominant pole in the pass-band was found to be:

For $t_0 = 10^{-10}$ s:

K	1.2	1.4	1.6	1.71
s_n	$-0.24485+j1.53$	$-0.13375+j1.61$	$-0.0396+j1.66$	$0+j1.69$

For $t_0 = 10^{-11}$ s:

K	0.8	1.0	1.2	1.327
s_n	$-0.2735+j1.02$	$-0.1466+j1.14$	$-0.0503+j1.22$	$0+j1.26$

For $t_0 = 10^{-12}$ s:

K	0.6	0.8	1.0	1.070
s_n	$-0.0695+j0.43$	$-0.0369+j0.50$	$-0.00855+j0.55$	$0+j0.57$

The system is unstable for $\sigma_n > 0$. It is seen that the delay, t_0, and the amount of feedback, g, thus significantly affect the graph of $|Z_1(j\omega)|$. A graph of the amplitude of the first-order photon response for $t_0 = 10^{-11}$ s, $K = 1.2$, and $I_1 = I_2 = 50$ ma, obtained using (15) is shown in Fig. 5. The plot is of $20\,\text{Log}_{10}(FP)$ vs. ω_n which is the magnitude in dB since this graph will be used later for determining the relative amplitudes of the various IMD components in dB.

It should be noted that the response maximum is inversely proportional to $|\sigma_n|$, the pole distance from the ω-axis. Consequently, for a given value of t_0, the response maximum increases monotonically with K so that the distortion increases with increasing K. To illustrate a relatively narrow pass-band case, all our examples below are for $t_0 = 10^{-11}$ s and $K = 1.2$.

3.1 IMD arising from the second-order Volterra operator

The response of the second-order Volterra operator is seen from (16) to contain only four non-zero frequency sinusoids. Each term varies as the square of the total input current amplitude but with a different dependence on I_1 and I_2. From Fig. 2, the IMD sinusoidal component with frequency $2\omega_1$ is seen to arise only from the product of two sinusoidal terms in which each term is the result of a linear operation on the input sinusoid with frequency ω_1. Consequently, the amplitude of this IMD component, SPR_1, varies as I_1^2 and is in-

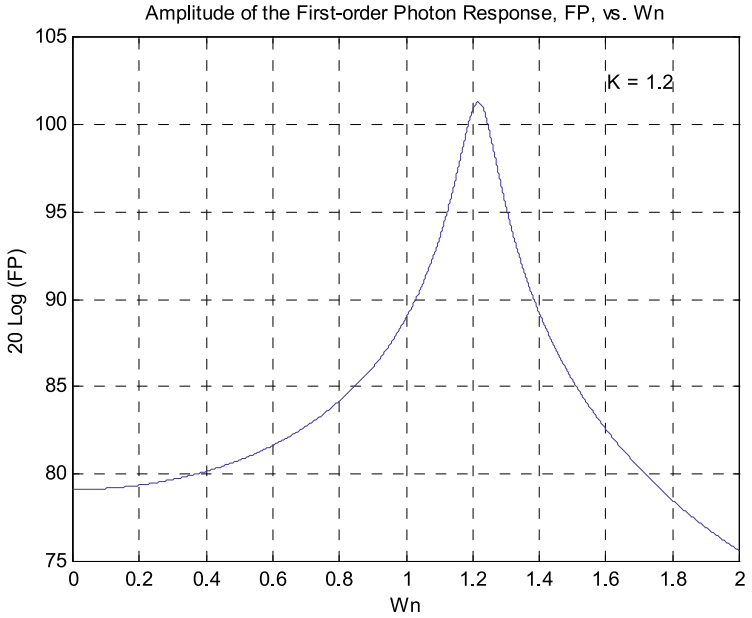

Fig. 5 Amplitude of the first-order photon response

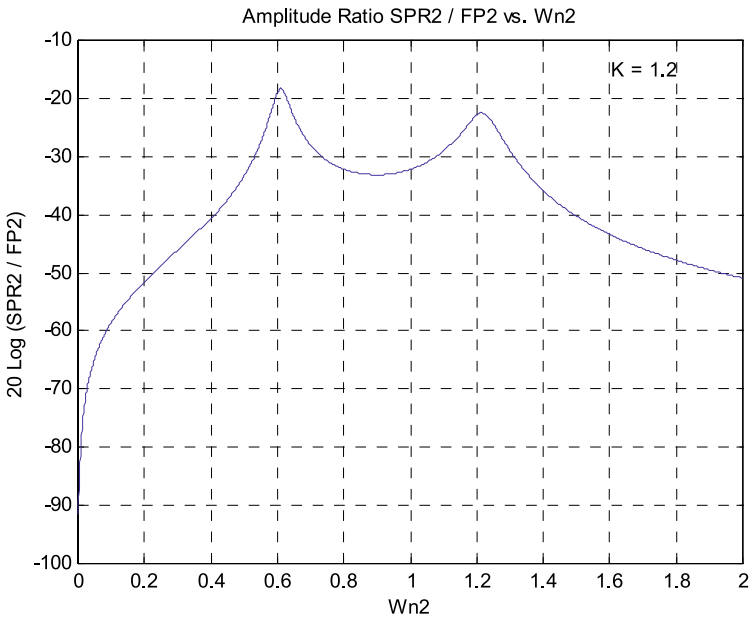

Fig. 6 Amplitude ratio SPR_2/FP_2 vs. ω_{n2}

dependent of I_2 so that the ratio $\frac{SPR_1}{I_1^2}$ is independent of the input current amplitude. Similarly, SPR_2, the amplitude of the IMD sinusoidal component with frequency $2\omega_2$ varies as I_2^2 and is independent of I_1 so that the ratio $\frac{SPR_2}{I_2^2}$ is independent of the input current amplitude. On the other hand, the sinusoid with frequency $(\omega_2 - \omega_1)$ is seen to arise from the product of two sinusoidal terms in which one term is the result of a linear operation on the input sinusoid with frequency ω_2, and the other term is the result of a linear operation on the input sinusoid with frequency ω_1.

Consequently, the amplitude of this IMD component, SPR_3, varies as $I_1 I_2$ so that the ratio $\frac{SPR_3}{I_1 I_2}$ is independent of the input current amplitude. Similarly, SPR_4, the amplitude of the IMD component with frequency $(\omega_2 + \omega_1)$ also varies as $I_1 I_2$ so that the ratio $\frac{SPR_4}{I_1 I_2}$ is independent of the input current amplitude. On the other hand, the exact variation of these IMD amplitudes with frequency is seen to depend on the transfer function of the linear systems involved. The shape of the graph of each of these IMD components vs. ω is thus affected by the feedback gain, g, and delay, t_0. A graph of the amplitude ratio of the second-order photon response, SPR_2 to FP_2 for $I_2 = 50$ ma, $K = 1.2$, and $t_0 = 10^{-11}$ s is shown in Fig. 6. The plot is of $20\,\mathrm{Log}_{10}(SPR_2/FP_2)$ vs. ω_{n2} so that the ordinate is the number of dB this IMD component differs from the first-order response amplitude. The

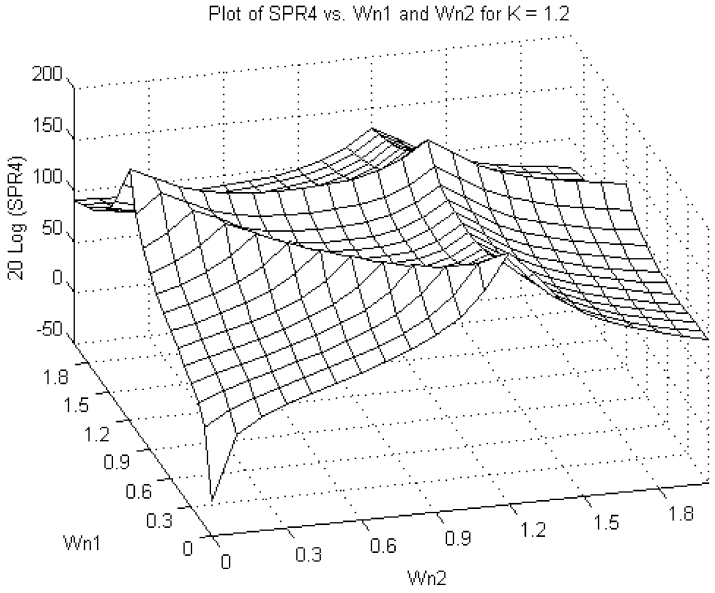

Fig. 7 Plot of SPR_4 vs. ω_{n1} and ω_{n2} for $K = 1.2$

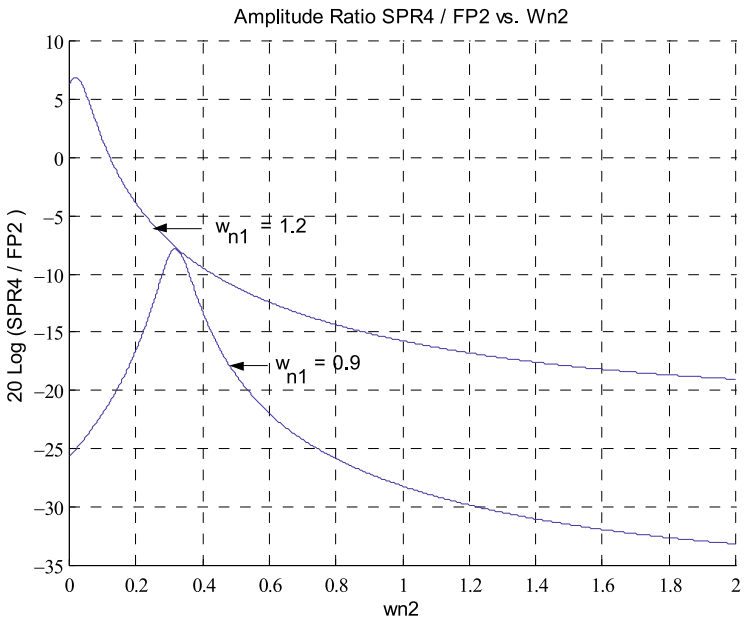

Fig. 8 Amplitude ratio SPR_4/FP_2 vs. ω_{n2}

peak at $\omega_{n2} = 1.2$ is due to the fact that the gain of the first linear system, R_1, in Fig. 1 has a maximum at $\omega_{n2} = 1.2$; the peak at $\omega_{n2} = 0.6$ results from the response to its second harmonic of the second linear system, R_1, in Fig. 1.

The IMD component amplitude SPR_2 depends only on the value of ω_2. However, the IMD component amplitude SPR_4 depends on both ω_1 and ω_2 as shown in Fig. 7 which is a three dimensional plot of $20\,\mathrm{Log}_{10}(SPR_4)$ vs. ω_{n1} and ω_{n2} for $I_1 = I_2 = 50$ ma, $t_0 = 10^{-11}$ s, and $K = 1.2$. It is seen that the shape of a graph of the ratio (SPR_4/FP_2) vs. ω_{n2} depends on the value of ω_{n1} used. A maximum value of SPR_4 occurs along the axis $\omega_{n1} = 1.2$. Figure 8 is a graph of the ratio (SPR_4/FP_2) vs. ω_{n2} for $\omega_{n1} = 0.9$ and 1.2.

Similarly, the IMD component with frequency $(\omega_2 - \omega_1)$ and amplitude, SPR_3 depends on both ω_1 and ω_2 as shown in Fig. 9 which is a three dimensional plot of $20\,\mathrm{Log}_{10}(SPR_4)$ vs. ω_{n1} and ω_{n2} for $I_1 = I_2 = 50$ ma, $t_0 = 10^{-11}$ s, and $K = 1.2$ so that the shape of a graph of the ratio (SPR_3/FP_2) vs. ω_{n2} also depends on the value of ω_{n1} used. A maximum of SPR_3 occurs along the axis $\omega_{n1} = 1.2$. Figure 10 is a graph of the ratio (SPR_4/FP_2) vs. ω_{n2} for $\omega_{n1} = 1.2$ and 1.4.

It should be noted that the second-order curves can be raised or lowered by changing the amplitude of the input. Since the amplitude of each term of the second-order response varies as the square of the total input current amplitude, the ratio of any second-order component to the input current amplitude varies as the amplitude of the total input

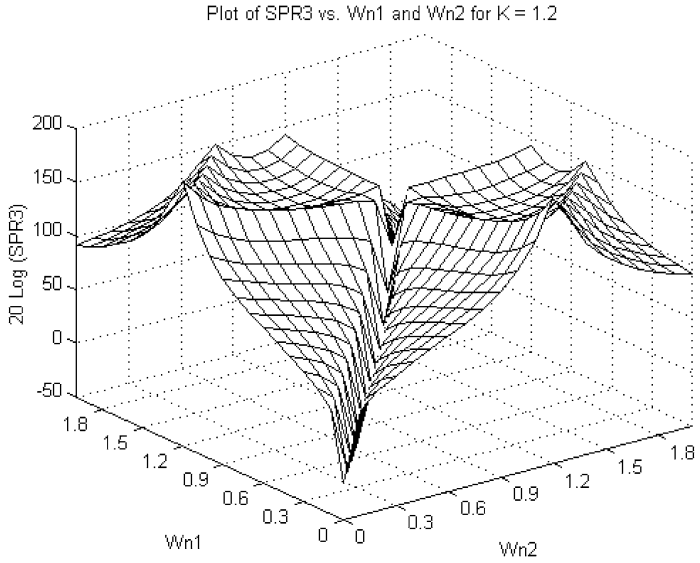

Fig. 9 Plot of SPR_3 vs. ω_{n1} and ω_{n2} for $K = 1.2$

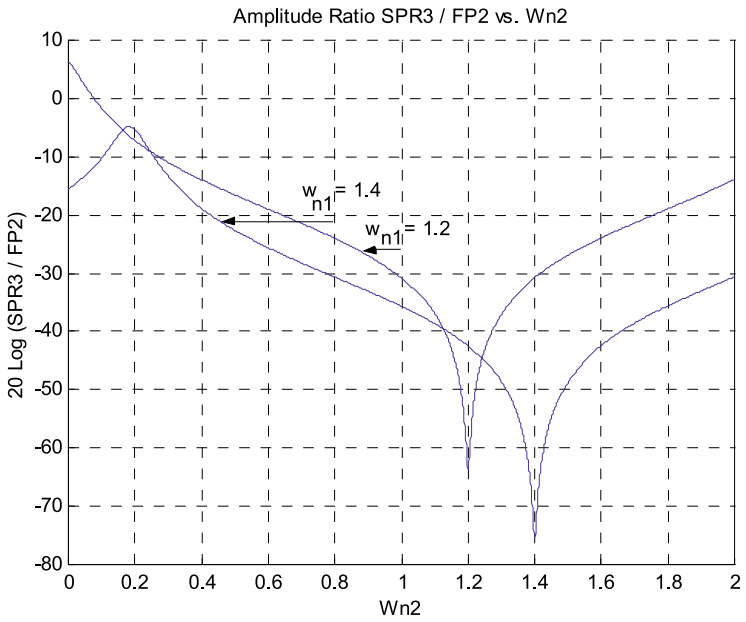

Fig. 10 Amplitude ratio SPR_3/FP_2 vs. ω_{n2}

current. Thus, if the total input current amplitude is changed by a factor of M, then the dB ratio of each second-order component to the total current amplitude will be changed by $20\,\mathrm{Log}_{10}(M)$. As an example, for an input current amplitude of 25 ma, the plots in Figs. 6, 8, and 10 will be the same except for a shift by an amount $20\,\mathrm{Log}_{10}(25/50) = -6.02$ dB.

3.2 IMD arising from the third-order Volterra operator

As is seen from (17), the response of the third-order Volterra operator contains eight non-zero frequency sinusoids. Each term varies as the cube of the total input current amplitude. However, their dependence on I_1 and I_2 is not as simple as in the case of second-order IMD since there are a number of different paths by which a given third-order IMD frequency term arises.

The various paths will have a different dependence on I_1 and I_2; the various possibilities are $I_1^m I_2^{(3-m)}$ for $m = 0, 1, 2$, and 3. For example, TPR_5, the amplitude of the sinusoid with frequency ω_2, is seen to arise from the following paths: (A) the product of the second-order term with frequency $2\omega_2$ with the first-order term with frequency ω_2, (B) the product of the second-order term with frequency $\omega_2 - \omega_1$ with the first-order term with frequency ω_1, (C) the product of the second-order term with frequency $\omega_2 + \omega_1$ with the first-order term with frequency ω_1, and (D) the product of the second-order term with zero frequency with the first-order term with frequency ω_2. The amplitude TPR_5 will thus be a linear combination of terms whose amplitudes

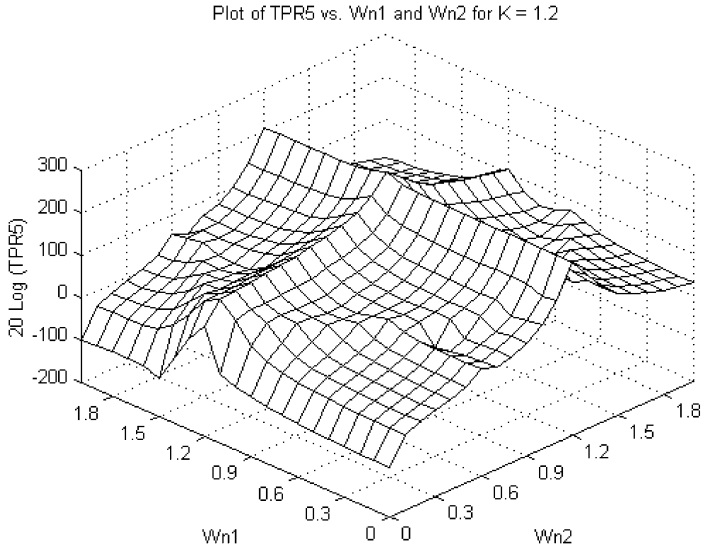

Fig. 11 Plot of TPR_5 vs. ω_{n1} and ω_{n2} for $K = 1.2$

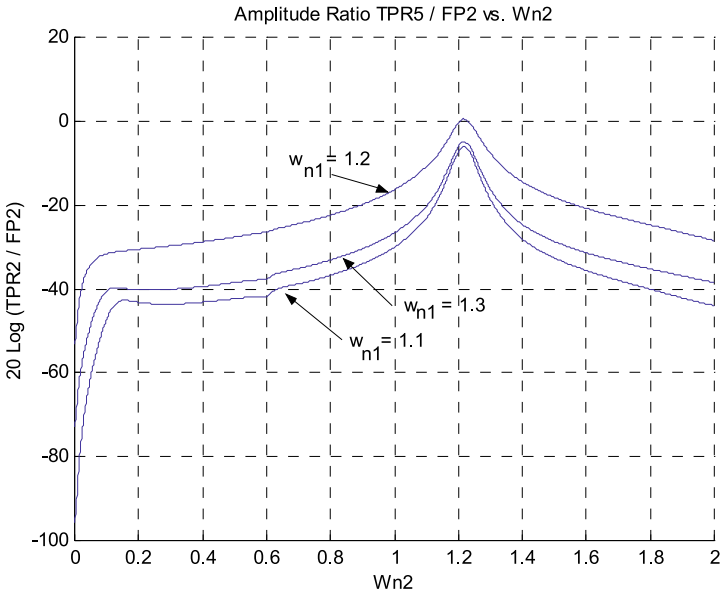

Fig. 12 Amplitude ratio TPR_5/FP_2 vs. ω_{n2}

vary as I_2^3 and $I_1 I_2^2$. Also, as with the second-order IMD, the exact variation of the third-order IMD amplitudes with frequency depends on the transfer function of the linear systems involved so that the graph of each of these IMD components is affected by the feedback gain, g, and delay, t_0.

From our discussion above, the third-order IMD component with frequency ω_2 and amplitude TPR_5 depends on both ω_1 and ω_2 as shown in Fig. 11 which is a three-dimensional plot of $20\,\mathrm{Log}_{10}(TPR_5)$ vs. ω_{n1} and ω_{n2} for $I_1 = I_2 = 50$ ma, $t_0 = 10^{-11}$ s, and $K = 1.2$. The shape of a graph of the ratio (TPR_5/FP_2) vs. ω_{n2} is seen to depend on the value of ω_{n1} used. Figure 12 is a graph of the ratio (TPR_5/FP_2) vs. ω_{n2} for $\omega_{n1} = 1.1, 1.2$, and 1.3.

The third-order IMD component with frequency $3\omega_2$ and amplitude TPR_7, however, is seen to arise only from the product of two sinusoidal terms; one which is the result of a linear operation on the input sinusoid with frequency ω_2 and the other which is the second-order IMD component with the frequency $2\omega_2$. Thus, the amplitude of this IMD component, TPR_7, varies as I_2^3 and is independent of I_1 so that the ratio $\frac{TPR_7}{I_2^3}$ is independent of the input current amplitude and also TPR_7 is independent of ω_1. Figure 13 is a plot of $20\,\mathrm{Log}_{10}(TPR_7/FP_2)$ vs. ω_{n2}.

The frequency of the IMD component with the amplitude TPR_{13} is $(2\omega_1 + \omega_2)$. The amplitude depends on both ω_1 and ω_2 as shown in Fig. 14 which is a three-dimensional plot of $20\,\mathrm{Log}_{10}(TPR_{13})$ vs. ω_{n1} and ω_{n2} for $I_1 = I_2 = 50$ ma, $t_0 = 10^{-11}$ s, and $K = 1.2$. As seen from Fig. 14, the shape of a graph of the ratio (TPR_{13}/FP_2) vs. ω_{n2} varies with the value of ω_{n1} used. This is illustrated in Fig. 15 which is a graph of the ratio (TPR_{13}/FP_2) vs. ω_{n2} for $\omega_{n1} = 0.01, 1.1$, and 1.2.

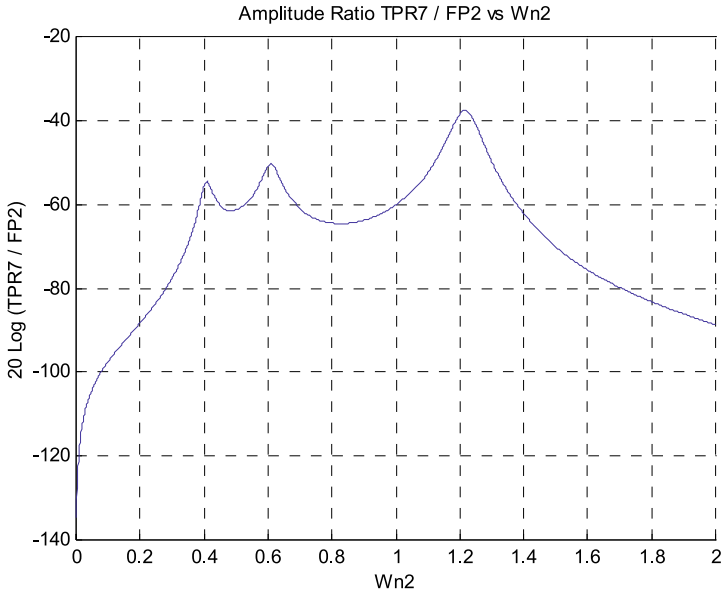

Fig. 13 Amplitude ratio TPR_7/FP_2 vs. ω_{n2}

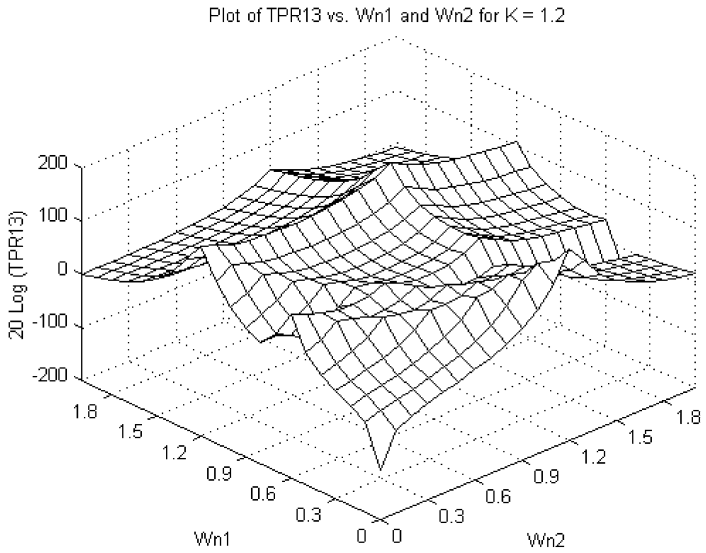

Fig. 14 Plot of TPR_{13} vs. ω_{n1} and ω_{n2} for $K = 1.2$

The frequency of the last third-order IMD component with the amplitude TPR_{19} is $(2\omega_1 - \omega_2)$. The amplitude depends on both ω_1 and ω_2 as shown in Fig. 16 which is a three-dimensional plot of $20\,\mathrm{Log}_{10}(TPR_{19})$ vs. ω_{n1} and ω_{n2} for $I_1 = I_2 = 50$ ma, $t_0 = 10^{-11}$ s, and $K = 1.2$. As seen from Fig. 16, the shape of a graph of the ratio (TPR_{19}/FP_2) vs. ω_{n2} varies with the value of ω_{n1} used. This is illustrated in Fig. 17 which is a graph of the ratio (TPR_{19}/FP_2) vs. ω_{n2} for $\omega_{n1} = 0.0, 0.6$, and 1.2.

As with the second-order IMD, the third-order IMD curves can be raised or lowered by changing the amplitude of the input. Since the amplitude of each term of the third-order response varies as the cube of the total input current amplitude, the ratio of any third-order component to the input current amplitude varies as the square of the input current amplitude. Thus, if the input current amplitude is changed by a factor of M, then the dB ratio of each third-order component to the total input current amplitude will be changed by $20\,\mathrm{Log}_{10}(M^2) = 40\,\mathrm{Log}_{10}(M)$. As an example, for an input current amplitude of 25 ma, the plots in Figs. 12, 13, 15, and 17 will be the same except for a shift by an amount $40\,\mathrm{Log}_{10}(25/50) = -12.04$ dB.

4 Conclusions

The Volterra model of the single-mode laser-diode developed in [1, 2] is useful for the determination and analysis of the laser-diode response to any given excitation. In this paper, it was used for the determination and analysis of the intermodulation distortion (IMD) of the single-mode laser-diode with electronic feedback. The output pho-

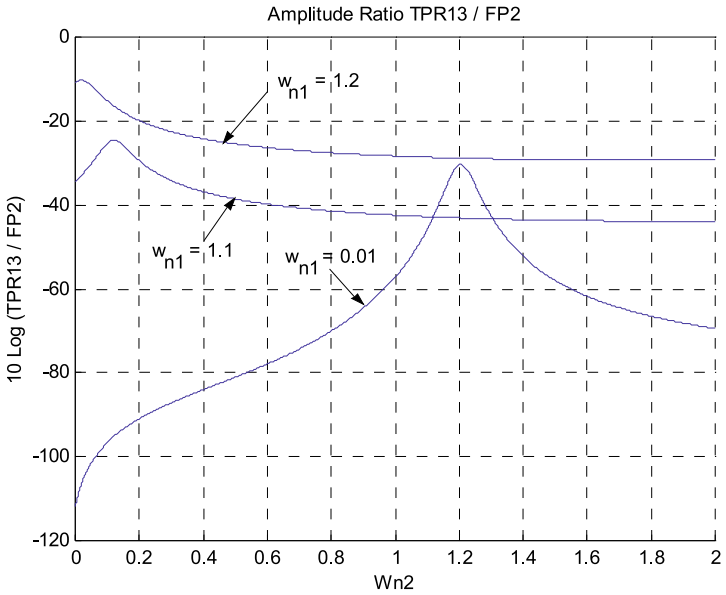

Fig. 15 Amplitude ratio TPR_{13}/FP_2

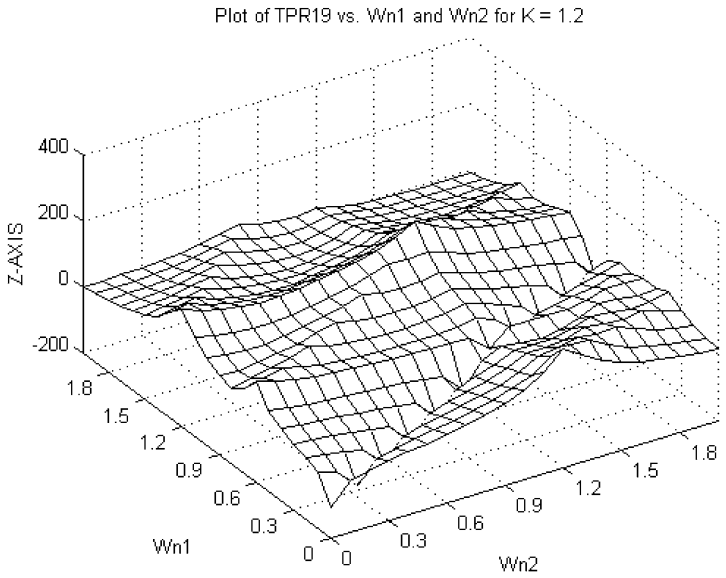

Fig. 16 Plot of TPR_{19} vs. ω_{n1} and ω_{n2} for $K = 1.2$

ton sinusoidal amplitudes resulting from the first-, second-, and third-order Volterra operators for an input which is the sum of two sinusoids were determined analytically from the Volterra model and programmed to obtain numerical results. These results allowed the study of the sources in the system model by which a given IMD component arises and also amplitude of each IMD component relative to the first-order photon output. As discussed in Sect. 3, the frequency response is determined by the feedback gain, K. To illustrate a relatively narrow pass-band case, all our examples were for $K = 1.2$. Lower values of IMD would be obtained for smaller values of K. Note from Fig. 12 that, for the parameter values used, the maximum amplitude of the third-order IMD component with a frequency which is the same as the input is approximately equal to that of the input's. This can be reduced by decreasing the total input current amplitude as discussed in Sect. 3.2. However, we also observe from this study the manner by which a larger gain of the first-order photon response increases the IMD amplitudes. Lowering the gain of the first-order linear system thus reduces the IMD amplitudes. This can be accomplished by decreasing the value of K to decrease the amount of feedback and/or increasing the feedback delay, t_0. The quantitative analysis on the dependency of an IMD amplitude on the input current that was presented can be used to determine the dB reduction of the IMD by this procedure.

The three-dimensional IMD graphs give insight of how the total IMD is affected by the input spectrum shape. Note that the shape of the three-dimensional graphs is determined by the Volterra kernels. Changing the feedback does re-

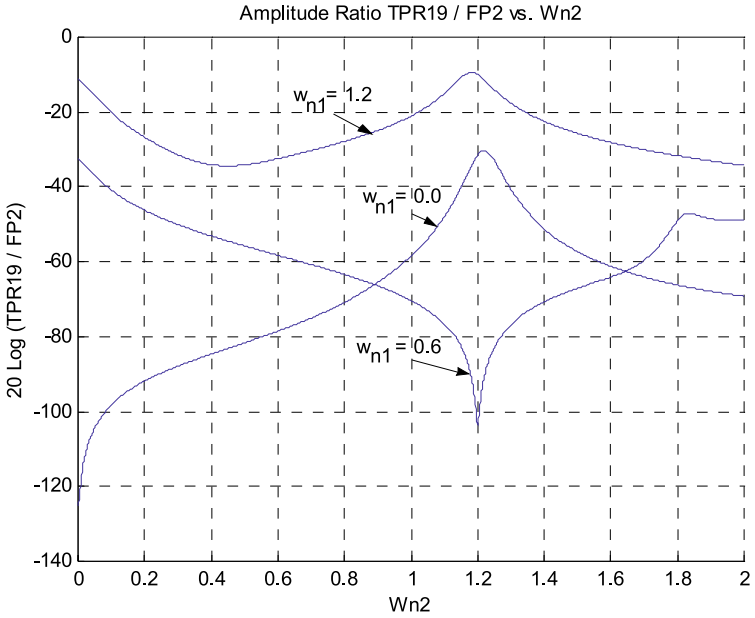

Fig. 17 Amplitude ratio TPR_{19}/FP_2 vs. ω_{n2}

sult in a change of the Volterra kernels and so the shape of the three-dimensional IMD graphs. The feedback can be changed by inserting a system in the feedback path. The desired system to use can be determined using the theory of nonlinear feedback systems developed in Sect. 8.5 of [2]. The insight obtained especially from the Volterra model of the manner by which various IMD components are formed thus greatly assists in the determination of ways by which its effects can be controlled.

In addition to the usefulness of the Volterra model in laser-diode IMD studies illustrated in this paper, it also can be used to determine and analyze the laser-diode response to any given excitation. The model also can be used for the determination of desirable values of the laser-diode parameters for a given application.

References

1. M. Schetzen, R. Yildirin, Opt. Commun. **219**, 341 (2003)
2. M. Schetzen, *The Volterra and Wiener Theories of Nonlinear Systems* (R.E. Krieger Publishing Co., Malabar, 2006)
3. R. Yildirin, M. Schetzen, Opt. Commun. **219**, 351 (2003)
4. M. Ohtsu, S. Kotajima, IEEE J. Quantum Electron. **21**, 1905 (1985)
5. G. Giacomeli, M. Calzavara, F.T. Arecchi, Opt. Commun. **74**, 97 (1989)
6. K. Sharaf, M.M. Ibrahim, IEEE J. Quantum Electron. **26**, 1347 (1990)
7. N.A. Loiko, A.M. Samson, Opt. Commun. **93**, 66 (1992)
8. C.H. Lee, S.Y. Shin, Appl. Phys. Lett. **62**, 922 (1993)
9. P. Sabourreau, J.P. Foing, P. Schanne, IEEE J. Quantum Electron. **33**, 1582 (1997)
10. T. Fukushima, T. Sakamoto, IEEE J. Quantum Electron. **34**, 750 (1998)
11. E.V. Grigorieva, H. Haken, S.A. Kaschenko, Opt. Commun. **165**, 279 (1999)
12. S. Tang, J.M. Liu, IEEE J. Quantum Electron. **37**, 1301 (2001)
13. H.D.I. Abarbanel, M.B. Kennel, I. Illing, H.F. Chen, J.M. Liu, IEEE J. Quantum Electron. **37**, 1301 (2001)
14. C. Juang, S.M. Chang, N.K. Hu, C. Lee, W.W. Lin, Jpn. J. Appl. Phys., Part 1 **44**, 7827 (2005)
15. G.Q. Xia, S.-C. Chan, J.-M. Liu, Opt. Express **15**, 572 (2007)
16. L. Hassine, Z. Toffano, F. Lamnabhi-Lagarrigue, A. Destrez, C. Birocheau, IEEE J. Quantum Electron. **30**, 918 (1994)